Int. J. Cancer: **107,** 1047–1052 (2003)

Publication of the International Union Against Cancer

NEAR-INFRARED RAMAN SPECTROSCOPY FOR OPTICAL DIAGNOSIS OF LUNG CANCER

Zhiwei HUANG[1], Annette MCWILLIAMS[1], Harvey LUI[2], David I. MCLEAN[2], Stephen LAM[1] and Haishan ZENG[1]*

[1]*Photomedicine and Optics Research Laboratory, Cancer Imaging Department, British Columbia Cancer Research Centre, Vancouver, British Columbia, Canada*

[2]*Photomedicine and Optics Research Laboratory, Division of Dermatology, University of British Columbia and Vancouver General Hospital, Vancouver, British Columbia, Canada*

Raman spectroscopy is a vibrational spectroscopic technique that can be used to optically probe the molecular changes associated with diseased tissues. The objective of our study was to explore near-infrared (NIR) Raman spectroscopy for distinguishing tumor from normal bronchial tissue. Bronchial tissue specimens (12 normal, 10 squamous cell carcinoma (SCC) and 6 adenocarcinoma) were obtained from 10 patients with known or suspected malignancies of the lung. A rapid-acquisition dispersive-type NIR Raman spectroscopy system was used for tissue Raman studies at 785 nm excitation. High-quality Raman spectra in the 700–1,800 cm^{-1} range from human bronchial tissues *in vitro* could be obtained within 5 sec. Raman spectra differed significantly between normal and malignant tumor tissue, with tumors showing higher percentage signals for nucleic acid, tryptophan and phenylalanine and lower percentage signals for phospholipids, proline and valine, compared to normal tissue. Raman spectral shape differences between normal and tumor tissue were also observed particularly in the spectral ranges of 1,000–1,100, 1,200–1,400 and 1,500–1,700 cm^{-1}, which contain signals related to protein and lipid conformations and nucleic acid's CH stretching modes. The ratio of Raman intensities at 1,445 to 1,655 cm^{-1} provided good differentiation between normal and malignant bronchial tissue ($p < 0.0001$). The results of this exploratory study indicate that NIR Raman spectroscopy provides significant potential for the noninvasive diagnosis of lung cancers *in vivo* based on the optic evaluation of biomolecules.

Key words: *bronchial tissue; lung cancer; near-infrared Raman spectroscopy; optic diagnosis*

Lung cancer is the second most common cancer in humans and is the most common cause of cancer deaths in the world. The overall 5-year survival rate of patients with lung cancer is no greater than 14%, which is much lower than that for patients with cancers in other organs, such as the bladder, breast, colon, cervix and prostate.[1] Early cancer detection and localization with effective treatment is crucial to increasing the survival rates. However, because early lung cancers or precancers such as dysplasia and carcinoma *in situ* (CIS) are only a few cell layers thick (0.2–1 mm), they can be very difficult to visually detect by conventional diagnostic methods. In the past decade, tissue fluorescence spectroscopy has been successfully used *in vivo* to diagnose early lung cancers.[2,3] Fluorescence point spectra may be collected in less than a second, and fluorescence imaging is possible due to the relatively high tissue autofluorescence that occurs in the lung.[4,5] Nevertheless, tissue autofluorescence spectral features are broad and show less specific differences between normal and pathologic tissues.[3] The Raman effect is an inelastic light scattering process whereby a very small proportion of incident photons are scattered (~1 in 10^8) with a corresponding change in frequency. The difference between the incident and scattered frequencies corresponds to the vibrational modes of molecules participating in the interaction. Raman spectra are depicted by plotting the intensity of the scattered photons as a function of the frequency shift. Raman spectra can capture a fingerprint of specific molecular species, and can therefore be potentially used for biomedic applications. Most biologic molecules are Raman-active scatterers, each with its own spectral fingerprint. Raman spectra usually exhibit sharp spectral features that are characteristic for specific molecular structures and conformations of tissue,[6,7] thus providing more specific molecular information about a given tissue or disease state.

Near-infrared (NIR) Raman spectroscopy has certain advantages, such as relative insensitivity to tissue water contents and deeper penetration depth into the tissue, that justify its increasing popularity for biomedic applications.[8–10] In recent years, NIR Raman spectroscopy has been investigated for *in vitro* diagnosis of malignant tissue from various organs (e.g., brain, breast, bladder, colon, larynx, cervix and skin).[8–16] These studies show that specific features of tissue Raman spectra can be related to the molecular and structural changes associated with neoplastic transformations.[17,18] A sensitivity and specificity of 82 and 92%, respectively, for differentiating between precancerous and benign cervic tissue *in vitro*, have been reported by Mahadevan-Jansen *et al.*[13] *In vivo* NIR Raman measurements have also been reported for the cervix, colon, esophagus and the skin.[19–22] However, Raman spectroscopy has not yet been applied to the bronchus to date.

Raman scattering from tissue is inherently very weak. It is very difficult to achieve measurements rapidly *in vivo* with a high signal-to-noise (S/N) ratio while avoiding interference from tissue autofluorescence and Raman signals from the silica fiber optics.[19,20,23] This is because the fiber-optic probes used to collect *in vivo* signals exhibit strong silica Raman scattering in the so-called fingerprint region (500–1,800 cm^{-1}). Moreover, data acquisition times and irradiance powers for *in vivo* use must be limited for practical and safety reasons. The primary goals of this exploratory study were to characterize NIR Raman spectra of bronchial tissues and to assess the possibility of using NIR Raman spectroscopy for optical diagnosis of lung cancers. Raman spectra of normal and malignant bronchial tissue were measured and compared, and the spectral differences between normal and tumor tissues were analyzed to test the diagnostic usefulness for lung cancer detection.

MATERIAL AND METHODS

Tissue specimens

A total of 28 bronchial tissue specimens were obtained from 10 patients (6 men and 4 women with a median age of 68.5 years) with clinically suspicious lesions or histologically proven malig-

Grant sponsor: National Cancer Institute of Canada; Grant sponsor: Canadian Dermatology Foundation.

*Correspondence to: Cancer Imaging Department, British Columbia Cancer Research Centre, 601 West 10th Avenue, Vancouver, B.C., V5Z 1L3, Canada. Fax: +1-604-877-6077 E-mail: hzeng@bccancer.bc.au

Received 22 January 2003; Revised 13 June 2003; Accepted 15 July 2003

DOI 10.1002/ijc.11500

nancies of the lung. All patients preoperatively signed an informed consent permitting the investigative use of tissues, and our study was approved by the Ethics Committee of the British Columbia Cancer Agency. Biopsies were taken from areas with abnormal fluorescence using fluorescence bronchoscopy with a Laser Imaging Fluorescence Endoscope (LIFE)–Lung device (Xillix Technologies Corp., Richmond, British Columbia, Canada).[24] After bronchoscopic biopsy or surgical resection, tissue specimens were placed in bottles with physiologic saline solution (pH = 7.4) and delivered to the laboratory for spectral studies within 30 min of biopsy or resection. The biopsy samples were approximately 1.5 × 1.5 × 1 mm in size, and to facilitate comparison of measurements, the surgically resected specimens were also cut into smaller sample sizes, similar to those of the biopsies. No sample pretreatment of any kind was performed prior to spectroscopic examination. After the NIR Raman measurement, the tissue samples were fixed in 10% formalin solution and then submitted for histopathologic examination. Pathologic evaluations showed that 12 specimens were normal, 6 were adenocarcinoma and 10 were squamous cell carcinoma (SCC). No necroses were found in any of the tumor tissue samples.

Raman instrumentation

Figure 1*a* shows a block diagram of the rapid-acquisition NIR Raman system we developed for tissue Raman spectroscopy measurements. This Raman system has a unique hardware design for improving S/N ratios by correcting the spectrograph image aberration so that good-quality tissue Raman spectra can be acquired rapidly (≤5 sec).[21] This dispersive-type Raman system consists of a diode laser emitting at 785 nm (maximum output, 300 mW; SDL Inc., San Jose, CA), a transmissive imaging spectrograph (HoloSpec-f/2.2-NIR, Kaiser Optical Systems Inc., Ann Arbor, MI) with a holographic grating (HSG-785-LF, Kaiser Optical Systems Inc., MI), an NIR-optimized, back-illuminated, deep-depletion charge-coupled device (CCD) detector (LN/CCD-EEV 1024 × 256, QE ≥ 75% at 900 nm; Princeton Instruments, Trenton, NJ) and a fiber-optic Raman probe (Fig. 1*b*).[21] The 785 nm laser is coupled to a 200 μm core diameter fiber (numerical aperture = 0.22), and the fiber is connected to the Raman probe via a subminiature version A (SMA) connector. The Raman probe was designed to maximize the collection of tissue Raman signals while reducing the interference of Rayleigh scattered light, fiber fluorescence and silica Raman signals. One optic arm of the probe consisting of a collimating lens, a bandpass filter (785 ± 2.5 nm) and a focusing lens delivers the laser light onto the tissue. The other optic arm of the probe equipped with collimating and refocusing lenses and a holographic notch plus filter (OD > 6.0 at 785 nm; Kaiser Optical Systems Inc., Ann Arbor, MI) is used for collecting tissue Raman signals. The holographic notch filter was placed between the 2 lenses to block the Rayleigh scattered excitation laser light while passing the frequency-shifted Raman signal. The refocusing lens then focused the filtered beam onto the circular end of the fiber bundle (58 × 100 μm core diameter fibers, NA = 0.22). Tissue Raman photons collected by the fiber bundle in the Raman probe are fed into the entrance of the transmissive spectrograph along a parabolic curve,[21] and the holographic grating disperses the incoming light onto the liquid nitrogen-cooled CCD array detector controlled by a PC. The combined autofluorescence and Raman spectra are displayed on the computer screen in real time and can be saved for further analysis. The system acquired spectra over the range 700–1,800 cm^{-1}, and each spectrum was acquired within 5 sec with light irradiance of 1.56 W/cm^2, which is less than the ANSI maximum permissible skin exposure limit for a 785 nm laser beam.[25] Raman frequencies were calibrated with the spectra of cyclohexane, acetone and barium sulfate to an accuracy of ± 2 cm^{-1} (the digital data resolution of the CCD detector). The spectral resolution of the system was 8 cm^{-1}. All spectra were corrected for the wavelength-dependent intensity response of the system using a standard lamp (RS-10, EG&G Gamma Scientific, San Diego, CA).

Data processing and analysis

The measured tissue spectra represented a combination of tissue Raman scattering, tissue autofluorescence and noise (Fig. 2). Therefore, the spectra were preprocessed by sequential 5-point

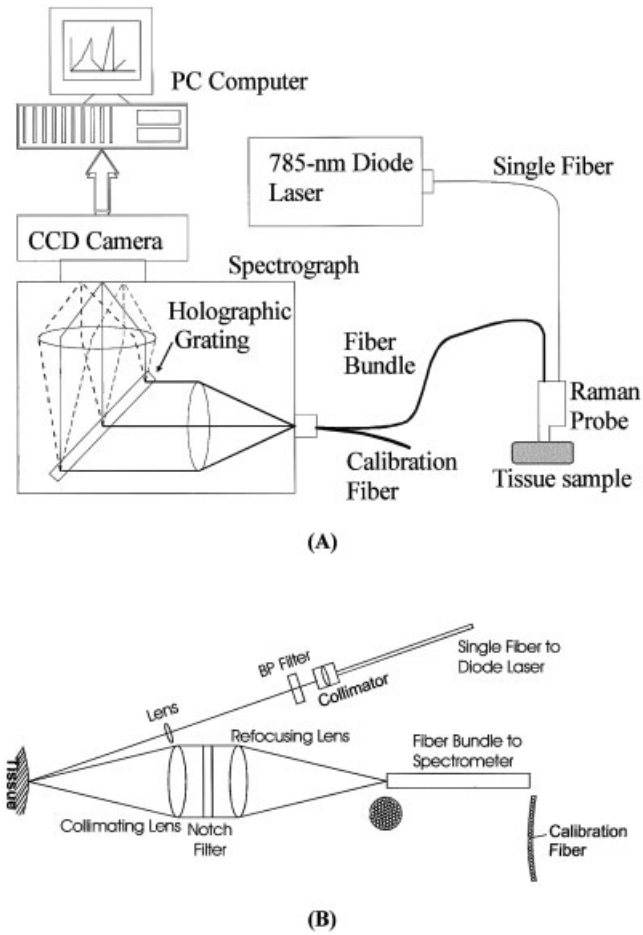

FIGURE 1 – *(a)* Block diagram of the rapid-acquisition NIR Raman spectrometer system used for tissue Raman measurements. CCD, charge-coupled device. *(b)* The fiber-optic Raman probe.

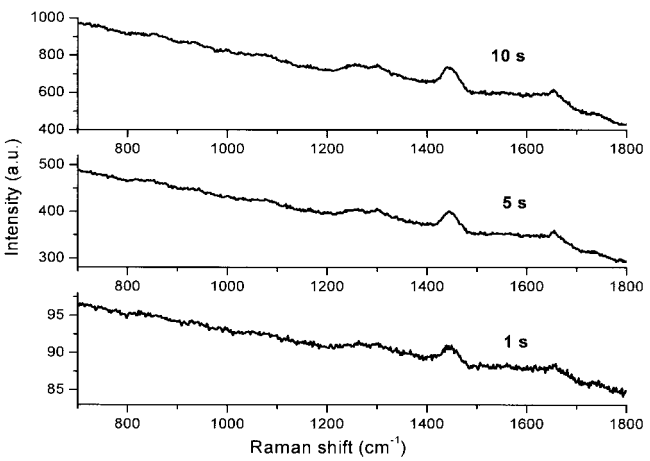

FIGURE 2 – Raman spectra from a normal bronchial tissue sample with signal acquisition times of 1, 5 and 10 sec, respectively. The spectra have been corrected for the spectral response of the system.

smoothing to reduce noise, and a fifth-order polynomial[13] was found to be optimal for fitting the autofluorescence background in the noise-smoothed spectrum over the range 700–1,800 cm^{-1}, excluding all regions with significant Raman spikes. This polynomial was subtracted from the measured spectrum to yield the tissue Raman spectrum alone. The overall intensity of the Raman spectra showed inter- and/or intrasample variations that also depended on the tissue sample size. Each of the tissue Raman spectra was therefore normalized or scaled by dividing by the total integral over the spectral range 700–1,800 cm^{-1}, enabling a better comparison of spectral patterns and percentage signals of various Raman bands between different tissue samples.

For the assessment of diagnostic sensitivity and specificity for tissue classification, histopathologic results were regarded as the gold standard. Normal and inflamed tissue were classified as benign or normal, whereas adenocarcinoma and SCC were classified as malignant. The unpaired Student's *t*-test (2-sided, equal variances) was used to test for differences between normal and malignant bronchial tissues, with respect to the mean value (mean ± SD) of the ratio of Raman intensity at 1,445 *vs.* 1,655 cm^{-1}.

RESULTS

Multiple spectra with different acquisition times were measured for each tissue sample. Figure 2 shows typical results for normal bronchial tissue using signal acquisition times of 1, 5 and 10 sec, respectively. It was evident that the spectrum of interest represented only a small contribution of tissue Raman scattering superimposed on an intense autofluorescence background. Increasing the acquisition time from 1 to 10 sec resulted in a corresponding increase in overall spectral intensity with improved S/N ratio, but no significant change in spectral shape. The results show that reproducible Raman spectra with high S/N ratios without interference from silica Raman signals from the fiber optics can be obtained within 5 sec with our rapid-acquisition Raman system.

To assess intrasample variability, multiple measurements (n = 10) on single samples of normal and tumor tissue were made at different regions of the samples and at different tissue orientations (epithelial and stromal sides of the tissue). There were no significant differences in the results obtained from different measurements of a given sample. Figure 3 shows the 5 sec Raman spectra without normalization as mean ± 1 SEM for normal tissue (*a*) and malignant (SCC) tissue (*b*), respectively. The overall spectral intensities varied by up to 12% about the mean for normal tissue, and up to 20% for tumor tissue. However, the relative Raman peak heights, shapes and positions showed little intrasample variability for either normal or tumor tissue. This finding has also been confirmed by background-subtracted Raman spectra (data not shown).

The effect of tissue specimen size on the Raman spectrum was also studied using one surgically resected normal specimen. This normal bronchial tissue was divided into 5 different samples with the dimensions listed in the legend to Figure 4, and the Raman probe was placed on the epithelial side of the tissue samples for Raman measurements. Figure 4*a* demonstrates how absolute signal intensities in the processed Raman spectra of normal bronchial tissue vary with specimen size (broadband autofluorescence background removed using a fifth-order polynomial fitting). The data show that absolute Raman intensity increased with sample size, although the Raman signal strength could be affected by *(i)* tissue inhomogeneity, *(ii)* tissue scattering and *(iii)* probe focusing on tissue sample. *In vivo* studies could help overcome signal variability due to different biopsy sizes. To correct for variations in absolute intensity, each of the Raman spectra in Figure 4*a* was normalized using the integrated area under the curve, and the y-axis was labeled as "normalized intensity" with unit "percentage (%) of total signals." This procedure greatly improved the reproducibility of the spectra for different specimen sizes, with intensity variations reduced to 10–20% for major Raman peaks (Fig. 4*b*).

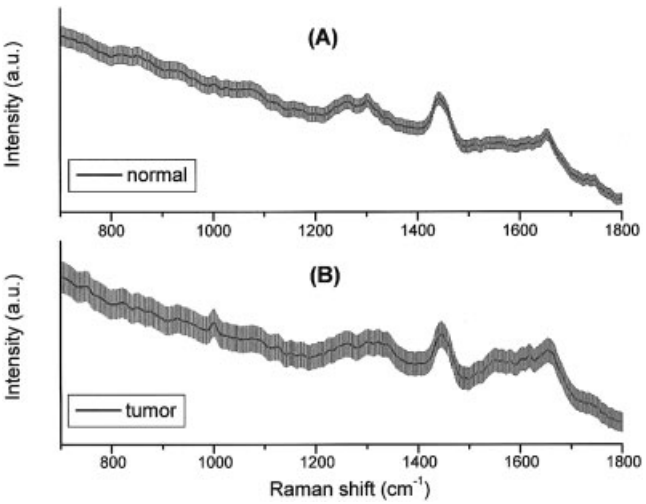

FIGURE 3 – Mean Raman spectra (solid line) ± 1 SEM (gray area) were obtained from single representative samples of normal tissue *(a)* and tumor *(b)* (SCC) by performing multiple measurements (n = 10) for each sample at different tissue orientations (epithelial and stromal sides of the tissue). All spectra were acquired in 5 sec with 785 nm excitation and corrected for the spectral response of the system.

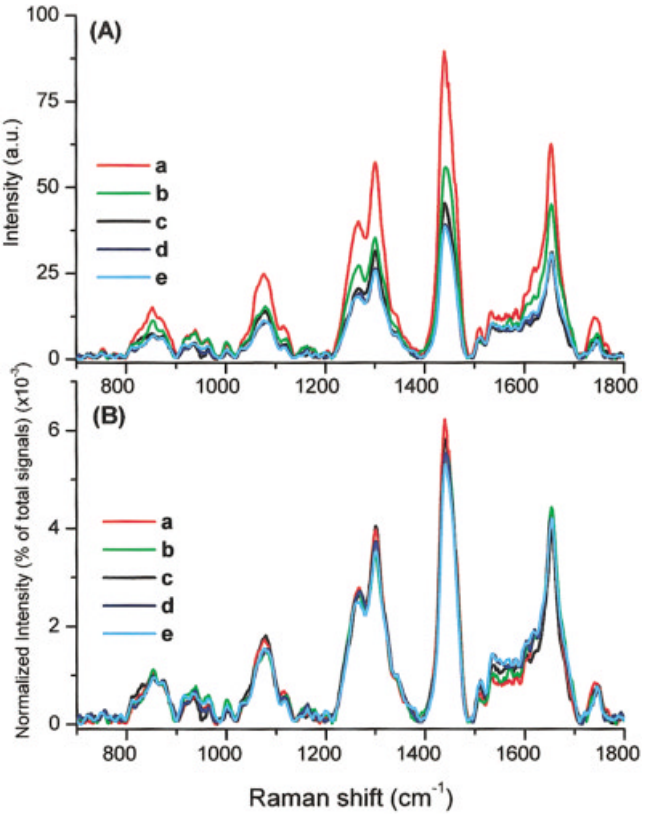

FIGURE 4 – Effect of varying specimen sizes on Raman spectra for normal bronchial tissue. *(a)* Before normalization for sample sizes: a) 8 × 8 × 1.5 mm; b) 5 × 5 × 1.5 mm; c) 4 × 4 × 1.5 mm; d) 3 × 3 × 1.5 mm; e) 1 × 1 × 1.5 mm. The larger specimen has a stronger Raman signal. *(b)* After normalization, all Raman spectra for different specimen sizes display almost identical patterns with intensity variations of 10–20% for major Raman peaks.

An exception to this general behavior can be seen in the region 1,500–1,600 cm^{-1}, where the ordering of signal intensity with smaller sample sizes was essentially reversed by the normalization procedure, probably due to artifact arising from water's contribution to the tissue Raman signals.[26] All tissue samples were kept moist with physiologic saline solution during Raman measurements. The smaller the sample, the more percentage of water adheres to the sample, and therefore, the higher the percentage of water that was sampled by the Raman probe.

Figure 5*a* shows the normalized mean Raman spectra of normal and malignant (adenocarcinoma and SCC) bronchial tissues. It can be seen that while significant Raman spectral differences exist between normal and tumor tissue, Raman spectra of adenocarcinoma are very similar to those of SCC with slight differences in the relative intensities of the 1,335, 1,445 and 1,655 cm^{-1} bands. Primary Raman peaks at 752, 823, 855, 876, 935, 1,004, 1,078, 1,123, 1,152, 1,172, 1,208, 1,265, 1,302, 1,335, 1,445, 1,518, 1,582, 1,618, 1,655 and 1,745 cm^{-1} can be consistently observed in both normal and tumor tissues, with the strongest signals at 1,265, 1,302, 1,445 and 1,655 cm^{-1}. The normalized intensities of Raman peaks at 855, 1,078, 1,265, 1,302, 1,445 and 1,745 cm^{-1} are greater for normal tissue than for tumor tissue, while Raman bands at 752, 1,004, 1,223, 1,335 and 1,550–1,620 cm^{-1} are more intense in tumor tissue. These normalized intensity differences can be viewed more clearly on the difference spectra between tumor and normal tissue (Fig. 5*b*). These difference spectra also revealed an increase in the Raman shoulder band at 1,668 cm^{-1} for tumor tissue.

The significant normalized Raman intensity differences between tumor and normal tissue result in differences in band shapes for the regions 1,000–1,100, 1,200–1,400 and 1,500–1,700 cm^{-1}. The bands for the regions 1,200–1,400 and 1,500–1,700 cm^{-1} appear broader for tumor tissue compared to normal tissue due to the enhanced intensity at 1,322 and 1,335 cm^{-1} and 1,552–1,618 cm^{-1} observed for tumor tissue. In addition, the peak positions at 1,078 and 1,265 cm^{-1} in normal tissue appear to have shifted to 1,088 and 1,260 cm^{-1}, respectively, in tumor tissue.

Figure 6 shows a scatter plot for the intensity ratio of I_{1445} *vs.* I_{1655} for each tissue sample, grouped according to tissue type (pathology). This ratio is >1 for 11/12 normal tissue samples and <1 for 15/16 tumor tissues. The mean value (mean ± SD) of this ratio for normal tissue (1.18 ± 0.15, $n = 12$) is significantly different from the mean ratio for all malignant tumor tissue samples tested (0.78 ± 0.13, $n = 16$) (unpaired Student's *t*-test, $p < 0.0001$). The decision line $I_{1445}/I_{1655} = 1$ separates tumor tissue from normal tissue with a sensitivity and specificity of 94% (95% confidence interval, 0.85–1.0) and 92% (95% confidence interval, 0.82–1.0), respectively.[27] In addition, the mean ratios for the 2 tumor types were 0.65 ± 0.05 (adenocarcinoma, $n = 6$) and 0.85 ± 0.09 (SCC, $n = 10$) respectively. Statistical analysis also shows that there are significant differences between the 2 tumor classes ($p < 0.0001$ for adenocarcinoma *vs*. SCC) and between each tumor type and normal tissue ($p < 0.0001$ for SCC *vs.* normal; $p < 0.0001$ for adenocarcinoma *vs.* normal).

DISCUSSION

Kaminaka *et al.*[28] recently reported preliminary results for Raman spectra from lung parenchyma with excitation at 1,064 nm. Background lung tissue autofluorescence can be significantly reduced as the excitation wavelength is shifted further into the NIR region. However, their measurements were done on lung samples soaked in formaldehyde solution rather than from fresh tissue, and it is known that formaldehyde fixation causes tissue changes and promotes the cross-linkage of amine groups in collagen, for example.[29] Thus, tissue fixation may cause significant changes in the Raman spectrum, especially in the amino acid fingerprint regions associated with proteins.[26,30] Such effects and their influences on the diagnostic potential of the Raman spectrum for lung cancer diagnosis warrant further study.

The results of our exploratory study demonstrated that there were specific differences in Raman intensities for malignant tumor

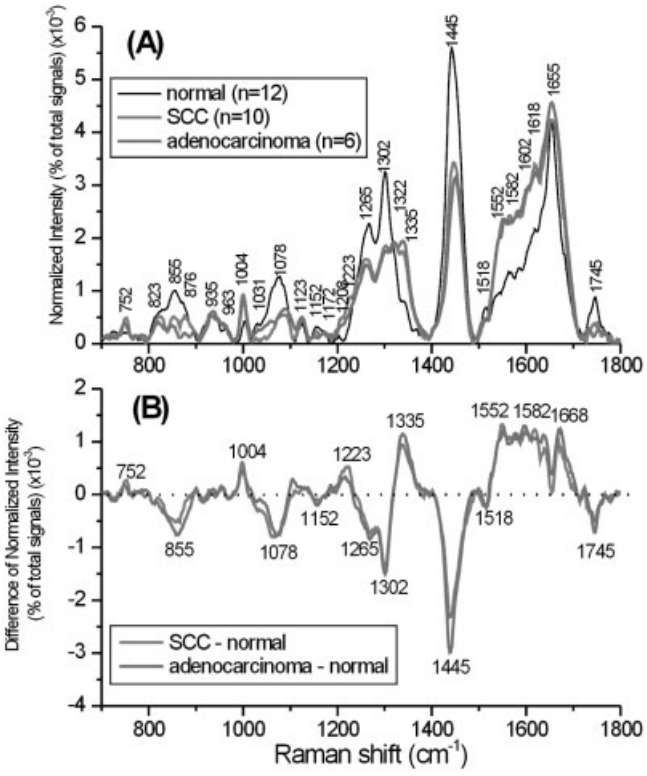

FIGURE 5 – *(a)*: The mean Raman spectra of normal bronchial tissue ($n = 12$) and malignant adenocarcinoma ($n = 6$) and SCC ($n = 10$) bronchial tissue samples. Each spectrum was normalized to the integrated area under the curve to correct for variations in absolute spectral intensity. *(b)* Difference spectra were calculated from the mean spectra: SCC minus normal and adenocarcinoma minus normal.

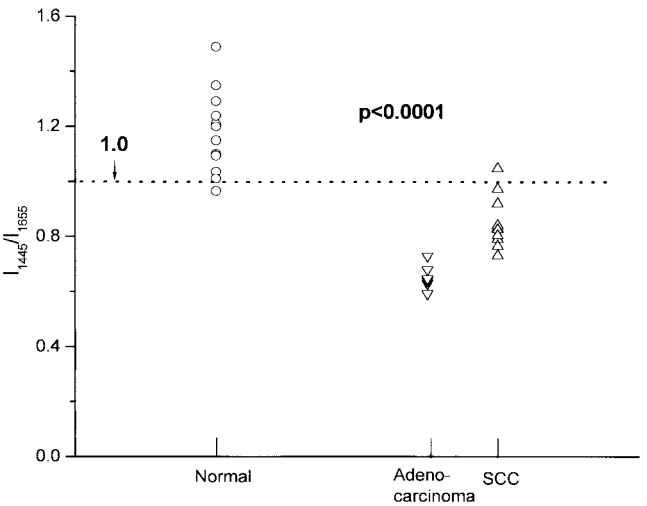

FIGURE 6 – Scatter plot of the intensity ratio of the Raman signal at 1,445 *vs.* 1,655 cm^{-1}, as measured for each sample and classified according to the histologic results. The mean ratio (1.18 ± 0.15) for normal tissue is significantly different ($p < 0.0001$) from the mean value (0.78 ± 0.13) for all tumor tissue (adenocarcinoma + SCC). The decision line ($I_{1445}/I_{1655} = 1$) separates tumor tissue from normal tissue with a sensitivity and specificity of 94% (95% confidence interval, 0.85–1.0) and 92% (95% confidence interval, 0.82–1.0).[27]

vs. normal tissue, confirming a potential role for NIR Raman spectroscopy in lung cancer diagnosis. In the range 700–1,800 cm^{-1}, Raman spectra of bronchial tissue are dominated by a number of vibrational modes of biomolecules, such as proteins, lipids and nucleic acids, which may be altered in quantity or form with neoplasia (Fig. 5*a*). To better understand the molecular basis for the observed Raman spectra of bronchial tissue, Table I lists tentative assignments for the observed Raman bands, according to literature data.[13–15,30–33] Thus, distinctive Raman features and intensity differences for tumor *vs.* normal bronchial tissue can reflect molecular and cellular changes associated with malignant transformation. For instance, the prominent Raman peaks at 1,265 and 1,655 cm^{-1}, respectively, in normal bronchial tissue can probably be attributed to the amide III and amide I bands of proteins in the α-helix conformation.[7] However, in malignant tissue, the amide III band was found to shift to 1,260 cm^{-1} and a shoulder band at 1,668 cm^{-1} (amide I) was also revealed in the difference spectra (Fig. 5*b*), suggesting that malignancy may be associated with an increase in the relative amounts of protein in the β-pleated sheet or random coil conformation.[18] The bands at 1,302 and 1,445 cm^{-1} are characteristic of the CH_2CH_3 bending modes of collagen and phospholipids,[12] and their percentage signals are considerably reduced in tumor tissue. The Raman bands of tryptophan (752, 1,208, 1,552 and 1,618 cm^{-1}) and phenylalanine (1,004, 1,582 and 1,602 cm^{-1}) in malignant tissue show higher percentage signals than those of normal tissue, indicating an increase in the percentage of tryptophan and phenylalanine contents relative to the total Raman-active components in tumor tissue. Brancaleon *et al.*[34] also observed an increase of tryptophan residues in skin tumor by fluorescence spectroscopy. However, the Raman bands for phospholipids at 1,078 and 1,745 cm^{-1}, proline at 855 cm^{-1}, and tyrosine at 823 and 855 cm^{-1} are much reduced in normalized intensity, indicating a decrease in the percentage of phospholipids relative to the total Raman-active constituents in tumor. The peak at 1,078 cm^{-1} in normal tissue due to the C–C or C–O stretching mode of phospholipids[32] was shifted to 1,088 cm^{-1} in tumor tissue and had lower normalized percentage signals, reflecting a decreased vibrational stability of lipid chains in tumors.[6] The strong Raman peak appearing at 1,322 and 1,335 cm^{-1} (CH_3CH_2 twisting and wagging in collagen)[32] in malignant tissue further confirmed the change of molecular structures of proteins in association with tumor transformations. On the other hand, Raman bands at 1,223 and 1,335 cm^{-1} due to cellular nucleic acids[6] in malignant tissues become widened and are greater than those of normal tissues, indicating that the percentage of nucleic acid contents relative to the total Raman-active components is much increased in tumor tissues. This is in agreement with histopathologic studies of grading malignancy by the nucleic acid-to-cytoplasm ratio.[35,36] These Raman peaks we observed in the bronchus have also been reported by NIR Raman spectroscopy in epithelia of other organs (e.g., larynx, cervix, colon and bladder).[12,13,15,30]

Bakker Schut *et al.*[37] used Raman microspectroscopy with 647 nm excitation to measure the intracellular carotenoid levels in lymphocytes of lung cancer patients and found a significant decrease of carotenoids for lung carcinoma patients compared to healthy subjects. In our study, the characteristic carotenoid Raman peaks at 1,152 and 1,518 cm^{-1} due to C–C and conjugated C=C bond stretch[38] were present in both normal bronchial and tumor tissue, but the normalized intensities of these peaks were reduced in tumor tissue. Our NIR Raman study on human bronchial tissue is in agreement with Bakker Schut *et al.*'s results. Carotenoids are thought to function as part of the tissue's antioxidant defense system.[33,39] Lower carotenoid levels in the bronchus may correlate with lung cancers,[37] and NIR Raman spectroscopy may be a novel method for studying the significance of the carotenoids in lung malignancies *in vivo*.

Simple but effective diagnostic algorithms have been proposed on the basis of the empirical analysis of Raman spectra in terms of peak intensity or peak intensity ratio measurements and have been applied to a number of organ types. For example, the ratio of intensities at 1,455 and 1,655 cm^{-1} has been used to classify tumor

TABLE I – PEAK POSITIONS AND TENTATIVE ASSIGNMENTS OF MAJOR VIBRATIONAL BANDS OBSERVED IN NORMAL AND TUMOR BRONCHIAL TISSUE.[13–15,30–33]

Peak position (cm^{-1})	Protein assignments	Lipid assignments	Others
1745w		ν (C═O), phospholipids	
1655vs	ν (C═O) amide I, α-helix, collagen, elastin		
1618s (sh)	ν (C═C), tryptophan		ν (C═C), porphyrin
1602ms (sh)	δ (C═C), phenylalanine		
1582ms (sh)	δ (C═C), phenylalanine		
1552ms (sh)	ν (C═C), tryptophan		ν (C═C), porphyrin
1518w			ν (C═C), carotenoid
1445vs	δ (CH_2), δ (CH_3), collagen	δ (CH_2) scissoring, phospholipids	
1335s (sh)	CH_3CH_2 wagging, collagen		CH_3CH_2 wagging nucleic acids
1322s	CH_3CH_2 twisting, collagen		
1302vs	δ (CH_2) twisting, wagging, collagen	δ (CH_2) twisting, wagging, phospholipids	
1265s (sh)	ν (CN), δ (NH) amide III, α-helix, collagen, tryptophan		
1223mw (sh)			$\nu_{as}(PO_2^-)$, nucleic acids
1208w (sh)	ν (C—C_6H_5), tryptophan, phenylalanine		
1172vw	δ (C—H), tyrosine		
1152w	ν (C—N), proteins		ν (C—C), carotenoid
1123w	ν (C—N), proteins		
1078ms		ν (C—C) or ν (C—O), phospholipids	
1031mw (sh)	δ (C—H), phenylalanine		
1004ms	ν_s, (C—C), symmetric ring breathing, phenylalanine		
963w	Unassigned		
935w	ν (C—C), α-helix, proline, valine		
876w (sh)	ν (C—C), hydroxyproline		
855ms	ν (C—C), proline δ (CCH) ring breathing, tyrosine		Polysaccharide
823w	Out-of-plane ring breathing, tyrosine		
752w	Symmetric breathing, tryptophan		

ν, stretching mode; ν_s, symmetric stretch; ν_{as}, asymmetric stretch; δ, bending mode; v, very; s, strong; m, medium; w, weak; sh, shoulder.

vs. normal tissue in the brain, breast, colon and cervix,[12,22] since both bands are sensitive to histologic abnormality.[8] Note that the 1,655 cm^{-1} band corresponds to the C=O stretching of collagen and elastin, and the 1,445 cm^{-1} band (CH_2 scissoring) varies with the lipid-to-protein ratio.[15,30,32] In our preliminary study with a small number of tissue samples, we also utilized this intensity ratio to distinguish malignant tumor tissue from normal bronchial tissue with a sensitivity and specificity of 94 and 92%, respectively (Fig. 6). The I_{1445}/I_{1655} was the largest for normal tissue (1.18 $\pm$ 0.15), significantly lower for SCCs (0.85 $\pm$ 0.09) and even lower for adenocarcinomas (0.65 $\pm$ 0.05). Further statistical analysis shows that the differences between the 2 tumor types and between each tumor type and normal tissue are also significant, although the sample populations are small in this preliminary study. Therefore, this intensity ratio is a potential diagnostic parameter for detecting and/or classifying different types of bronchial malignancies. Note that the simplistic empirical analysis employed here used only 2 Raman peaks for tissue classification; most of the information contained in the Raman spectra has not been used. Therefore, a multivariate statistical analysis (e.g., principal components analysis (PCA)),[13,23] which utilizes the entire spectrum and automatically determines the most diagnostically significant features (factors), may improve the efficiency of the method for tissue analysis and classification. Currently, we are performing Raman measurements on samples from a larger patient series, and PCA and cross-validation techniques will be applied to the database when the sample size is sufficiently large. If a miniaturized fiber-optic Raman probe[40] were successfully developed to interface with our rapid-acquisition Raman system for the collection of Raman signals via endoscope, NIR Raman spectroscopy could become a potentially useful clinical tool for rapid and noninvasive diagnosis of lung cancers *in vivo* based on probing changes at the molecular level. This technique may also be a useful adjunct to conventional bronchoscopy for guiding and directing biopsies for histopathologic investigation of lung malignancies.

REFERENCES

1. Greenlee RT, Hill-Harmon MB, Murray T, Thun M. Cancer statistics. CA Cancer J Clin 2001;51:15–36.
2. Lam S, Kennedy T, Unger M, Miller YE, Germont D, Rusch V. Localization of bronchial intraepithelial neoplastic lesions by fluorescence bronchoscopy. Chest 1998;113:696.
3. Hung J, Lam S, LeRiche JC, Palcic B. Autofluorescence of normal and malignant bronchial tissue. Lasers Surg Med 1991;11:99–105.
4. Lam S, MacAulay C, Hung J, LeRiche J, Profio AE, Palcic B. Detection of dysplasia and carcinoma in situ with a lung imaging fluorescence endoscope device. J Thorac Cardiovasc Surg 1993;105:1035–40.
5. Zellweger M, Grosjean P, Goujon D, Monnier P, van den Bergh H, Wagnieres G. *In vivo* autofluorescence spectroscopy of human bronchial tissue to optimize the detection and imaging of early cancers. J Biomed Opt 2001;6:41–51.
6. Perno JR, Grygon CA, Spiro TG. Raman excitation profiles for the nucleotides and for the nucleic acid duplexes poly(rA)-poly(rU) and poly(dG-dC). J Phys Chem 1989;93:5672–8.
7. Tu AT. Peptide backbone conformation and microenvironment of protein side chains. In: Clark RJH, Hester RE, eds. Spectroscopy of biological systems. New York: John Wiley & Sons, 1986. 13:47–112.
8. Frank CJ, McCreery RL, Redd DC. Raman spectroscopy of normal and diseased human breast tissues. Anal Chem 1995;67:777–83.
9. Manoharan R, Shafer K, Perelman L, Wu J, Chen K, Deinum G, Fitzmaurice M, Myles J, Crowe J, Dasari R, Feld MS. Raman spectroscopy and fluorescence photon migration for breast cancer diagnosis and imaging. Photochem Photobiol 1998;67:15–22.
10. Schrader B, Keller S, Loechte T, Fendel S, Moore DS, Simon A, Sawatzki J. NIR FT Raman spectroscopy in medical diagnosis. J Mol Struct 1995;348:293–6.
11. Lawson EE, Barry BW, Williams AC, Edwards HGM. Biomedical applications of Raman spectroscopy. J Raman Spectrosc 1997;28:111–7.
12. Liu CH, Das BB, Glassman WL, Tang GC, Yoo KM, Zhu HR, Akins DL, Lubicz SS, Cleary J, Prudente R, Celmer E, Caron A, et al. Raman, fluorescence and time-resolved light scattering as optical diagnostic techniques to separate diseased and normal biomedical media. J Photochem Photobiol Biol 1992;16:187–209.
13. Mahadevan-Jansen A, Mitchell MF, Ramanujam N, Malpica A, Thomsen S, Utzinger U, Richards-Kortum R. Near-infrared Raman spectroscopy for *in vitro* detection of cervical precancers. Photochem Photobiol 1998;68:123–32.
14. Mizuno A, Kitajima H, Kawauchi K, Muraishi S, Ozaki Y. Near-infrared Fourier transform Raman spectroscopic study of human brain tissues and tumors. J Raman Spectrosc 1994;25:25–9.
15. Stone N, Stavroulaki P, Kendall C, Birchall M, Barr H. Raman spectroscopy for early detection of laryngeal malignancy: preliminary results. Laryngoscope 2000;110:1756–63.
16. Lau DP, Huang Z, Lui H, Man CS, Berean K, Morrison MD, Zeng H. Raman spectroscopy for optical diagnosis in normal and cancerous tissue of the nasopharynx—preliminary findings. Lasers Med Surg 2003;32:210–4.
17. Alfano RR, Liu CH, Sha WL, Zhu D, Akins L, Cleary J, Prudente R, Cellmer E. Human breast tissues studied by IR Fourier transform Raman spectroscopy. Lasers Life Sci 1991;4:23–8.
18. Mahadevan-Jansen A, Richards-Kortum R. Raman spectroscopy for the detection of cancers and precancers. J Biomed Opt 1996;1:31–70.
19. Mahadevan-Jansen A, Mitchell MF, Ramanujam N, Utzinger U, Richards-Kortum R. Development of a fiber optic probe to measure NIR Raman spectra of cervical tissue *in vivo*. Photochem Photobiol 1998; 68:427–31.
20. Shim MG, Wong LKS, Marcon NE, Wilson BC. *In vivo* near-infrared Raman spectroscopy: demonstration of feasibility during clinical gastrointestinal endoscopy. Photochem Photobiol 2000;72:146–50.
21. Huang Z, Zeng H, Hamzavi I, McLean D, Lui H. Rapid near-infrared Raman spectroscopy system for real-time *in vivo* skin measurements. Opt Lett 2001;26:1782–4.
22. Utzinger U, Heintzelman DL, Mahadevan-Jansen A, Malpica A, Follen M, Richards-Kortum R. Near-infrared Raman spectroscopy for *in vivo* detection of cervical precancers. Appl Spectrosc 2001;55:955–9.
23. Bakker Schut TC, Witjes MJ, Sterenborg HJ, Speelman OC, Roodenburg JL, Marple ET, Bruining HA, Puppels GJ. *In vivo* detection of dysplastic tissue by Raman spectroscopy. Anal Chem 2000;72:6010–8.
24. Lam S, MacAulay C, LeRiche JC, Palcic B. Detection and localization of early lung cancer by fluorescence bronchoscopy. Cancer 2000; 89(Suppl):2468–73.
25. ANSI 2136.1-1986, American National Standard for the Safe Use of Lasers. Washington, D.C.: American National Standards Institute, 1986.
26. Huang Z, McWilliams A, Lam S, English J, McLean D, Lui H, Zeng H. Effect of formalin fixation on the near-infrared Raman spectroscopy of human bronchial tissues. Int J Oncol 2003; 23:649–55.
27. Fleiss JL. Statistical methods for rates and proportions, 2nd ed. New York: Wiley & Sons, 1981;13–8.
28. Kaminaka S, Yamazaki H, Ito T, Kohda E, Hamaguchi H. Near-infrared Raman spectroscopy of human lung tissues: possibility of molecular-level cancer diagnosis. J Raman Spectrosc 2001;32:139–41.
29. Bloom W, Fawcett DW. A textbook of histology. Philadelphia: W.B. Saunders, 1980;121–67.
30. Shim MG, Wong LKS, Marcon NE, Wilson BC. The effects of ex vivo handling procedures on the near-infrared Raman spectra of normal mammalian tissues. Photochem Photobiol 1996;63:662–71.
31. Keller S, Schrader B, Hoffmann A, Schrader W, Metz K, Rehlaender A, Pahnke J, Ruwe M, Budach W. Application of near-infrared Fourier transform Raman spectroscopy in medical research. J Raman Spectrosc 1994;25:663–71.
32. Dollish FR, Fateley WG, Bentley FF. Characteristic Raman frequencies of organic compounds. New York: Wiley, 1974;215–83.
33. Hata TR, Scholz TA, Ermakov IV, McClane RW, Khachik F, Gellermann W, Pershing LK. Non-invasive Raman spectroscopic detection of carotenoids in human skin. J Invest Dermatol 2000;115:441–8.
34. Brancaleon L, Durkin AJ, Tu JH, Menaker G, Fallon JD, Kollias N. *In vivo* fluorescence spectroscopy of nonmelanoma skin cancer. Photochem Photobiol 2001;73:178–83.
35. Naber SP. Molecular pathology: detection of neoplasia. N Engl J Med 1994;331:1508–10.
36. Steitz TA. Structural studies of protein-nucleic acid interaction: the sources of sequence-specific binding. Q Rev Biophys 1990;23:205–80.
37. Bakker Schut TC, Puppels GJ, Kraan YM, Greve J, van der Maas LL, Figdor CG. Intracellular carotenoid levels measured by Raman microspectroscopy: comparison of lymphocytes from lung cancer patients and healthy individuals. Int J Cancer 1997;74:20–5.
38. Koyama Y, Takasuka I, Nakata M, Tasumi M. Raman and infrared spectra of the all-trans, 7-cis, 9-cis, 13-cis and 15-cis isomers of carotene: key bonds distinguishing stretched or terminal-bent configurations from central-bent configurations. J Raman Spectrosc 1998;19:37–49.
39. McMillan DC, Talwar D, Sattar N, Underwood M, St J O'Reilly D, McArdle C. The relationship between reduced vitamin antioxidant concentrations and the systemic inflammatory response in patients with common solid tumours. Clin Nutr 2002;21:161–4.
40. Shim MG, Wilson BC, Marple E, Wach M. Study of fiber-optic probes for *in vivo* medical Raman spectroscopy. Appl Spectrosc 1999;53:619–27.